Polyrotaxane-based thin film composite membranes for enhanced nanofiltration performance

Min Liu,[1] Mitchell D. Nothling,[1] Shereen Siew Tan,[1] Paul A. Webley,[1] Greg G. Qiao,[1] Qiang Fu[1,2]**

[1]Department of Chemical Engineering, The University of Melbourne, Parkville, VIC, 3010, Australia.

[2]The Centre for Technology in Water and Wastewater (CTWW), the School of Civil and Environmental Engineering, University of Technology Sydney (UTS) NSW 2007 Australia.

Abstract: An urgent need exists for the development of advanced water purification technologies to meet the increasing global demand being placed on freshwater resources. Membrane-based separation technologies for size-selective contaminant removal represent a promising approach to achieve this goal. Here, a novel thin film composite nanofiltration membrane is prepared *via* interfacial polymerization of α-cyclodextrin on a commercially available polyacrylonitrile substrate. Subsequent *in-situ* inclusion complexation of alkyne-functionalized poly(ethylene glycol) (PEG) is then used to tune the polyrotaxane-based pores for size-dependent filtration. The resultant membrane shows excellent size-selective rejection rates for organic dye (*e.g.* rhodamine B, >99%) as well as heavy-metal ions (*e.g.* Co(II), >90%), while crucially maintaining high water permeance (*e.g.* H_2O: 7.1 L h^{-1} m^{-2} bar^{-1}). The facile and straightforward synthetic approach to the fabrication of polyrotaxane nanofiltration membranes, combined with their strong nanofiltration

separation performance, holds significant promise for membrane-based water purification applications.

Keywords: α-cyclodextrin, poly(ethylene glycol), polyrotaxane, thin film composite membrane, nanofiltration

***Corresponding Authors:**

Greg G. Qiao: gregghq@unimelb.edu.au.

Qiang Fu: qiang.fu@uts.edu.au

1. Introduction

The global demand for access to clean water is predicted to increase by 55% over the next 25 years, exasperated by rapid population growth, increasing urbanisation and climate change [1]. Meeting this demand requires overcoming the challenge of water contamination by industrial processes, impacting the availability of existing water resources. The urgent development of advanced water purification technologies is therefore an imperative goal for further research. Within this domain, conventional phase-change processes for molecular separation exhibit high water purification rates [2], however, their associated high energy demand limits their economic and environmental feasibility. In contrast, high-performance membrane systems have the potential to realize energy-efficient separation/purification processes using an effective single-step barrier, which has motivated intense recent study in the development of novel membrane systems [3]. Among these designs, composite nanofiltration membranes (with pore sizes <2 nm) are particularly attractive due to their ability to simultaneously remove most organic dyes and inorganic contaminants from diverse water sources [2, 3].

Currently, most nanofiltration membranes suffer from a well-known trade-off: *i.e.* increasing membrane permeance results in reduced selectivity (contaminant rejection rate), and *vice versa* [4]. As a result, a key challenge in the fabrication of high-performance composite nanofiltration membranes has been to maximize the permeation rate (*i.e.* permeance) while maintaining high selectivity toward a target solute. An effective approach to enhance membrane separation performance is to reduce the thickness and/or increase the diffusion free volume of selective layers. To achieve this, pristine ordered microporous materials such as metal organic frameworks (MOFs) and covalent organic frameworks (COFs) with defined cavity shapes and sizes have been employed for the fabrication of ultrapermeable and highly selective membranes [5-9]. For

example, a crystalline 2D COF membrane was prepared on an Anodisc aluminium oxide support, where the resultant membranes gave a molecular weight cut-off (MWCO) of *ca.* 900 Da and exhibited a 100-fold increase in polar/non-polar solvent permeability compared with their amorphous counterparts [5]. Similarly, the Vankelecom group reported a polyethersulfone supported ZIF-8 membrane prepared *via* an interfacial synthesis method, with the membranes offering high water permeance (155.9 kg m^{-2} h^{-1} bar^{-1}) and good rejection rates of 92.5% for rhodamine B (RB, Molecular Weight: 479.02 Da) [10]. Given pristine MOF or COF membranes have shown superior water purification performance in laboratory settings, issues with their stability, flexibility, and ease of processing have limited their potential uptake by industry. In addition, due to the relatively large pore size of these materials, the fabricated membranes usually display good performance in the ultrafiltration range but the targeted rejection of metal ions by nanofiltration (< 2 nm) is currently unachievable. Conversely, polymeric materials (*e.g.* polyamide) have been used for nanofiltration membranes for several decades [11]. However, their relatively low free volume restricts their permeability, impacting on separation permeance. This led us to pose the following question: can a selective membrane material be realized with a high rejection rate while maintaining good solvent permeance for both organic molecules and inorganic metal ions?

Cyclodextrins (CDs) are a promising candidate for membrane construction due to their nontoxic, intrinsically porous structure, and large-scale commercial availability. Indeed, CDs have also been widely used to prepare water purification membranes through radical polymerization or copolymerization with flexible polymers [12-19]. The resultant CD membranes showed high stability, flexibility, and good separation performance in the ultrafiltration range. However, extending their performance into nanofiltration applications has so far proven challenging [16, 19,

20]. To fully exploit the potential of the CD-based membranes, we further introduce a polymer 'axle' into CD's cavity, affording a polyrotaxane (PRX)-based composite membrane employing tuneable inter-/intra- CD pores for nanofiltration. The membranes are prepared *via* a straightforward interfacial polymerization (IP) method (Scheme 1i, ii), followed by *in-situ* inclusion complexation of poly(ethylene glycol) (PEG) into the CD cavity and end-capping reaction to lock the filtration construct (Scheme 1iii, iv). The resultant PRX membranes show significantly enhanced rejection rates for both organic dyes and heavy metal ions, while maintaining high solvent permeance in comparison with pristine CD membranes.

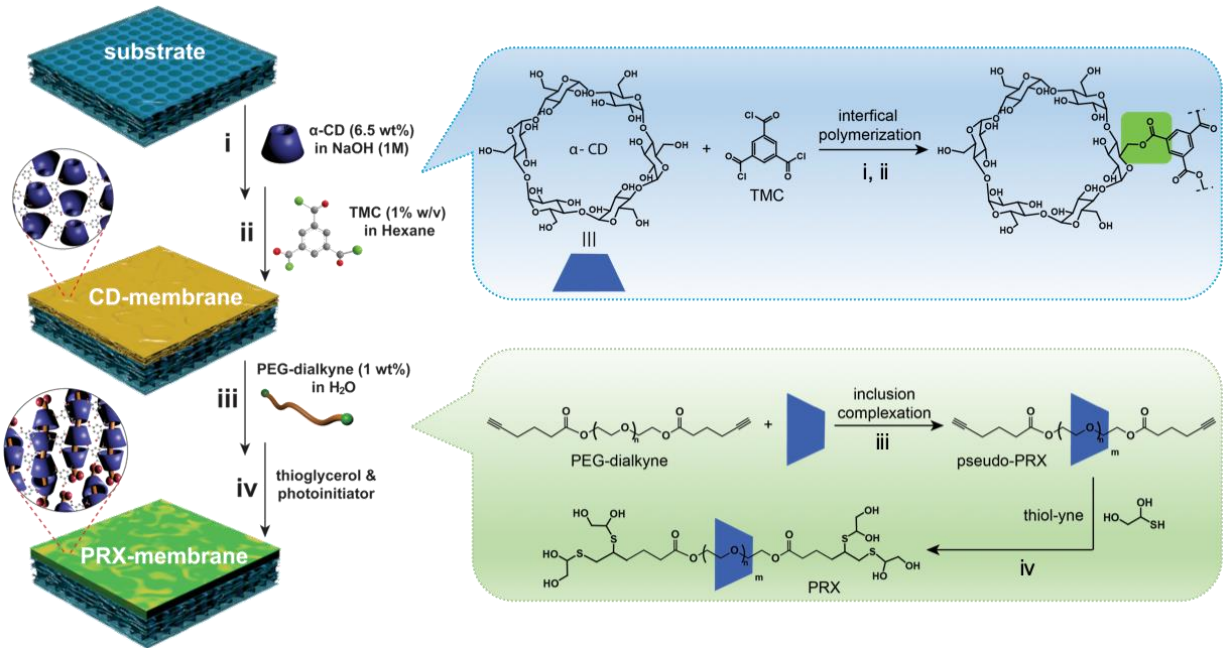

Scheme 1. Preparation of polyrotaxane (PRX)-based composite nanofiltration membranes. Interfacial polymerization (IP) on polyacrylonitrile (PAN) substrates pre-wetted with ethanol by sequentially immersing the substrates in: (i) 1 M NaOH solution containing 6.5 wt% of *α*-cyclodextrin (*α*-CD); (ii) hexane solution containing 1% w/v trimesoyl chloride (TMC); (iii) *in-situ* inclusion complexation of *α*-CD and alkyne-terminated polyethylene glycol (PEG-dialkyne),

and; (iv) end-capping *via* a thiol-yne 'click' chemistry using thioglycerol and photo-initiator under UV irradiation (λ = 365 nm).

2. Experimental

2.1 Materials

α-Cyclodextrin (α-CD) (Aldrich, 98%) was dried in vacuo (0.1 mbar, 70 °C) for 12 h immediately prior to use. Trimesoyl chloride (TMC, 95%), 1-thioglycerol (97%), *N,N,N′,N″,N″*-pentamethyldiethylenetriamine (PMDETA, 99%), sodium ascorbate, 4-(phenylazo)benzoic acid (98%), copper(II) sulfate pentahydrate ($CuSO_4 \cdot 5H_2O$, 99.9%), ruthenium(III) chloride ($RuCl_3$, Ru content 45-55%), silver nitrate ($AgNO_3$, ≥99%), cobalt(II) nitrate hexahydrate ($Co(NO_3)_2 \cdot 5H_2O$, 98%), tris[2-(dimethylamino)ethyl]amine (Me_6TREN, 97%), and nickel(II) nitrate tetrahydrate ($Ni(OCOCH_3)_2 \cdot 4H_2O$, 98%) were purchased from Aldrich and used as received. The water-soluble photo initiator lithium phenyl-2,4,6-trimethylbenzoyl-phosphinate was purchased from Tokyo Chemical Industry Co. Ltd. and used as received. Methanol (MeOH, 99.8%), ethanol (EtOH, 99.5%), isopropanol (IPA, >99.5%), AR grade sodium hydroxide (NaOH) and hexane (anhydrous, 95%) were purchased from Chem-Supply and used without further purification. Polyacrylonitrile (PAN) microporous support (MWCO = 10 kDa) was purchased from SolSep BV. Alkyne functionalized poly(ethylene glycol) (PEG-dialkyne) precursors with different molecular weights (M_n = 2,000, 4,000 and 10,000 g mol^{-1}) were synthesized according to a previous report and characterization by 1H NMR and MALDI confirmed the target structures (Fig. 1) [21].

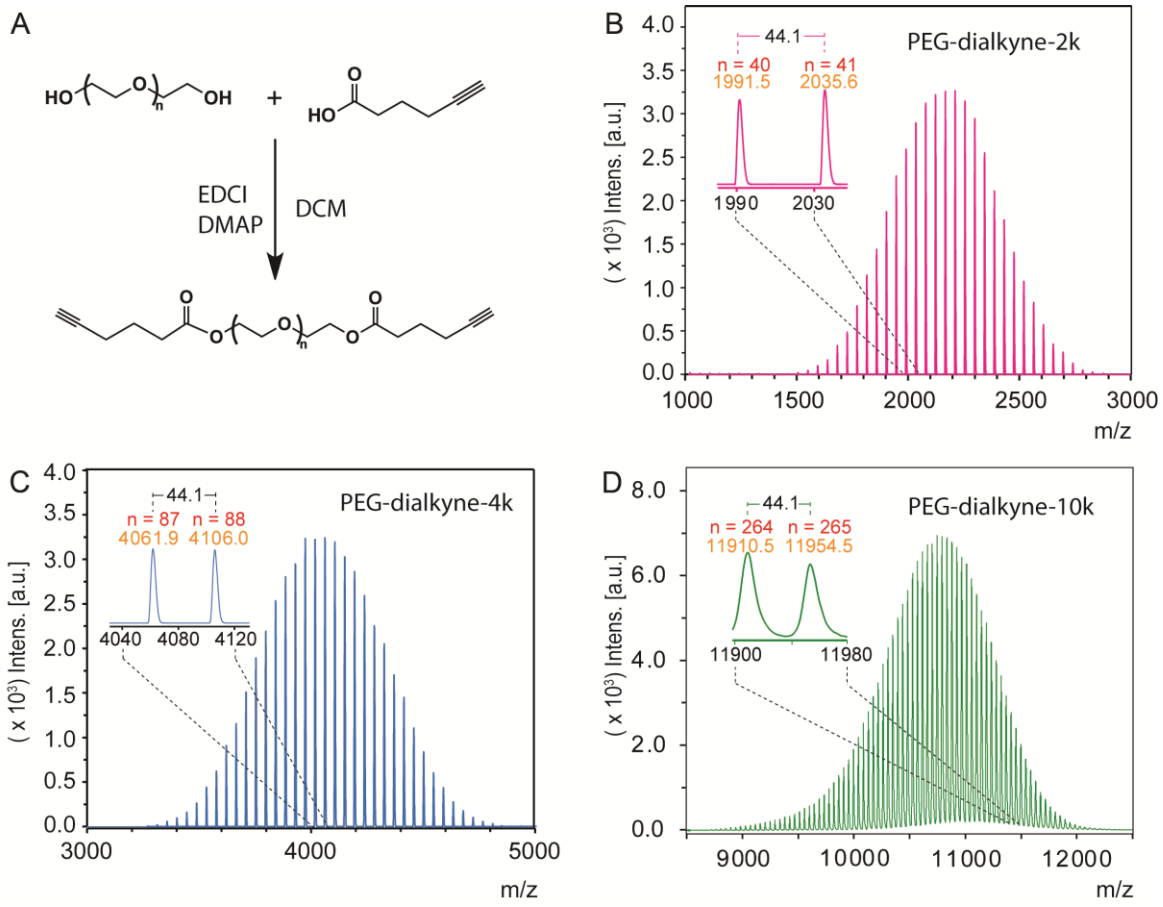

Fig. 1. (A) Schematic illustration of the preparation of PEG-dialkyne precursors. (B-D) MALDI-ToF MS of the prepared PEGs with molecular weights of 2,000, 4,000 and 10,000 g mol^{-1}, respectively. ^{1}H NMR (400 MHz, d_6-DMSO): d_H 4.14–4.11 (m, 2H, -C*H*$_2$OCO-), 3.69–3.30 (m, 4H, -C*H*$_2$C*H*$_2$O-), 2.80 (t, *J* = 2.8 Hz, 1H, -C≡C*H*), 2.40 (t, *J* = 7.2 Hz, 2H, -C*H*$_2$COO-), 2.20 (dt, *J* = 2.8 and 7.2 Hz, 2H, ≡CC*H*$_2$-), 1.69 (quin, *J* = 7.2 Hz, 2H, -C*H*$_2$-) ppm.

2.2 Methods

Synthesis of α-Cyclodextrin (CD) Films: Cyclodextrin (CD) membranes were prepared following conditions reported in the literature [16]. Firstly, a commercial porous PAN membrane was immersed in a 6.5% (w/v) of *α*-cyclodextrin (*α*-CD) NaOH (1 M) aqueous solution for 30 min (Scheme 1i). Next, the cyclodextrin loaded PAN support was wiped with tissue to remove excess

solution from the surface. Then, the surface of the PAN support was exposed to a 1% (w/v) of TMC in hexane solution for 10 min (Scheme 1ii). Finally, the membrane was washed with hexane to remove the unreacted TMC, dried for at least 12 hours at room temperature, rinsed and stored in DI water.

Preparation of Polyrotaxane (PRX) Membranes: As a representative protocol, the polyrotaxane (PRX) membranes were prepared *via* an *in-situ* inclusion complexation (Scheme 1iii), followed by an end-capping reaction (Scheme 1iv). Specifically, the prepared CD membranes were immersed in PEG-dialkyne aqueous solution (2 mM) at room temperature for 12 hours with stirring. Then, the membranes were washed with DI water 3 times to remove un-complexed PEG. The resultant membranes were immersed in an aqueous solution containing 1-thioglycerol (10 mM) and lithium phenyl-2,4,6-trimethylbenzoyl-phosphinate (0.15 mM). The film was then exposed to UV irradiation (365 nm, 4 × 12 W) to induce the end-capping *via* thiol-yne 'click' chemistry. After 4 hours, the obtained membranes were washed with DI water, dried for 12 hours at room temperature, rinsed and stored in DI water.

Nanofiltration Performance: A series of liquid phase permeation experiments were conducted with a vacuum filtering device and the prepared PRX membranes. The permeation rate of water or organic solvents and rejection rate of metal ions or dye molecules were evaluated (effective membrane area = 9.62 cm^2). All experiments were done at room temperature and repeated at least three times. All membranes were preconditioned in the solvent by permeating it for at least 1 hour before taking any measurements. The solute concentration used in the tested solutions was 50 ppm for metal ions, 10 ppm for 4-(phenylazo)benzoic acid and 2.5 ppm for rhodamine B. The analysis of the solute concentration was determined by using either UV-vis spectrophotometer for the dyes and Ru^{3+} and Cu^{2+} ions, or ICP-OES for Ag^{2+}, Co^{2+}, and Ni^{2+} metal ions. Of particular note, a few

drops of Me_6TREN was added into the permeated Cu^{2+} solution to allow for the formation of a stable complex before the UV-vis measurements were conducted.

2.3 Characterization

Nuclear Magnetic Resonance (^{1}H NMR) spectroscopy were conducted on a Varian Unity 400 MHz spectrometer operating at 400 MHz, using the sample concentrations of approximately 10 mg mL^{-1}. Matrix-assisted laser desorption/ionization time of flight mass spectroscopy (MALDI-ToF MS) was performed on a Bruker Autoflex III Mass Spectrometer operating in positive linear mode; the analyte, matrix (trans-2-[(tert-butyl-phenyl)-2-methyl-2-propenylidene]-malononitrile, DCTB, 98+%, Santa Cruz Biotechnology) and cationization agent (sodium trifluoroacetate, NaTFA, 98%, Aldrich) were dissolved in THF at a concentration of 10 mg mL^{-1}, and then mixed in a volume ratio of 1:10:1. Then, 0.3 μL of this solution was spotted onto a ground steel target plate and the solvent was allowed to evaporate prior to analysis. Flex Analysis (Bruker) was used to analyse the data. Scanning Electron Microscopy (SEM) measurements were conducted on a Quanta FEG 200 ESEM. Samples were coated with gold using a Dynavac Mini Sputter Coated prior to imaging. The membrane cross-sections were observed by transmission electron microscopy (TEM), scanning transmission electron microscope (STEM) and energy-dispersive X-ray spectroscopy (EDX) mapping using FEI Tecnai F20 microscope. Samples were coated with carbon and platinum prior to cut by focused ion beam (FIB). X-ray photoelectron spectroscopy (XPS) analysis was performed on a VG ESCALAB 220i-XL spectrometer under ultra-high vacuum (6×10^{-9} mbar) to reveal the surface composition of the TFC membrane. A fixed photon energy (Al Kα 1486.6 eV) was used. A survey scan was performed between 0 and 1200 eV with a resolution of 1.0 eV and pass energy of 100 eV. High resolution scans for C 1s, O 1s and S 2p were also conducted with a resolution of 0.05 eV and a pass energy of 20 eV. X-ray diffraction

(XRD) patterns of the samples were recorded on a Bruker D8 Advance instrument with Cu Kα radiation (40 kV, 40 mA) and a nickel filter, and the samples were exposed at a scanning rate of $2\theta = 0.02° \cdot s^{-1}$ in the range of 3-70°. Attenuated total reflectance infrared (ATR-FTIR) spectroscopy was performed on a Nexus 470 Fourier-Transform Infrared Spectrometer (Thermo Nicolet). The ICP-OES was performed on a Perkin Elmer Optima 4300 DV using calibration curves generated from standard solutions (0.1-50 ppm). UV-vis absorbance spectra were obtained using Shimadzu UV-1800 spectrophotometer and UV Probe software package.

3. Results and discussion

3.1 Membrane Characterization

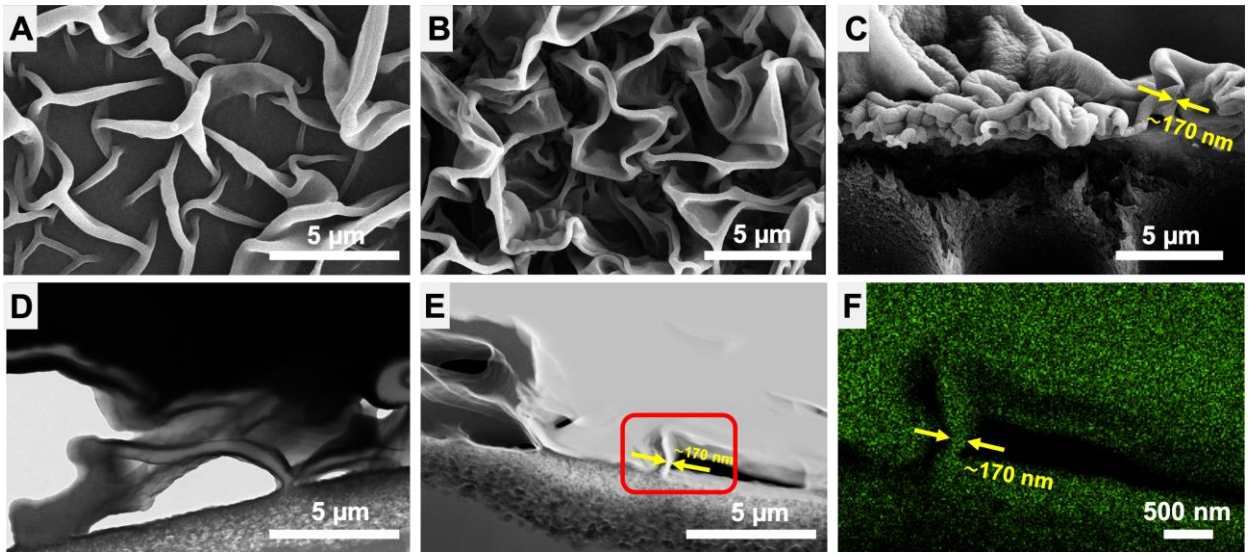

Fig. 2. Scanning electron microscopy (SEM) images of (A) the CD membrane and (B, C) polyrotaxane-4k (PRX-4k) membrane (top and cross-section view, respectively). Cross-sectional (D) transmission electron microscopy (TEM) and (E) scanning transmission electron microscope (STEM) images of the PRX-4k membrane. (F) Energy-dispersive X-ray spectroscopy (EDX) mapping image of the red region in (E), highlighting the thin PRX selective layer.

To prepare the PRX membranes, alpha-cyclodextrin (α-CD) was firstly cross-linked with a trimesoyl chloride (TMC) crosslinker to create a thin CD layer on commercially available polyacrylonitrile (PAN) substrates *via* a conventional IP method (Scheme 1, steps i-ii). α-CD (I.D. 5.7 Å) was selected over alternative CD ring sizes due to its high inclusion complexation index with polyethylene glycol (PEG), leading to the formation of a stable *pseudo*-polyrotaxane [22, 23]. The resultant CD membrane displayed a surface composed of microscale wrinkles visible by scanning electron microscopy (SEM) (Fig. 2A). Such "crumpled" morphology is advantageous for membrane applications due to an enhanced fluid contact area compared with smooth/flat membranes. In addition, analysis of the membrane by attenuated total reflection–Fourier transform infrared spectroscopy (ATR-FTIR) revealed the characteristic C-O (1026 cm^{-1} and 1350 cm^{-1}) vibration of CD, as well as the *Ar*-vibrations at 1613 cm^{-1} and 1569 cm^{-1} and the C=O (1716 cm^{-1}) vibration of TMC, providing strong evidence for the successful preparation of α-CD membranes (Fig. 3A).

Next, complete nanofiltration PRX membranes were fabricated by inclusion complexation of alkyne functionalized PEG within the CD layer (Scheme 1, step iii), followed by an end-capping reaction with thioglycerol (Scheme 1, steps iv). The inclusion of PEG was expected to narrow the pore size of the α-CD membrane and therefore enhance the rejection rate towards small organic molecules and inorganic heavy metal ions. Of particular note, the PEG chains were permanently locked in the complexation structure after the 'thiol-yne' end-capping reaction. PEG-dialkyne with different molecular weights would display different hydrodynamic diameters (as 'random-coil') in aqueous media, which in turn affect their diffusivity during the inclusion complexation with α-CDs. As a result, three alkyne-terminated PEG precursors with different molecular weights (2000, 4000, and 10,000 g mol^{-1}, Fig. 3) were employed to investigate the inclusion effect on membrane

performance. Interestingly, no clear increase in membrane thickness after PEG inclusion was observed *via* SEM analysis (Fig. 2A and B). Furthermore, the formed PRX layer displayed a thickness of ~170 nm (Fig. 2C), suggesting a folded morphology of the wrinkles observed on the membrane surface in Fig. 2B. To confirm the ultrathin feature of the prepared PRX membrane, the PRX-4k membrane was cut by focused ion beam (FIB) and imaged by TEM, STEM, and EDX mapping (Fig. 2D-F). The cross-sectional TEM image shows a crumpled morphology (Fig. 2D), agreeing well with parallel SEM analysis. The EDX mapping image of the red region in Fig. 1E highlights the ultrathin nature (~170 nm) of an unfolded PRX-4k layer.

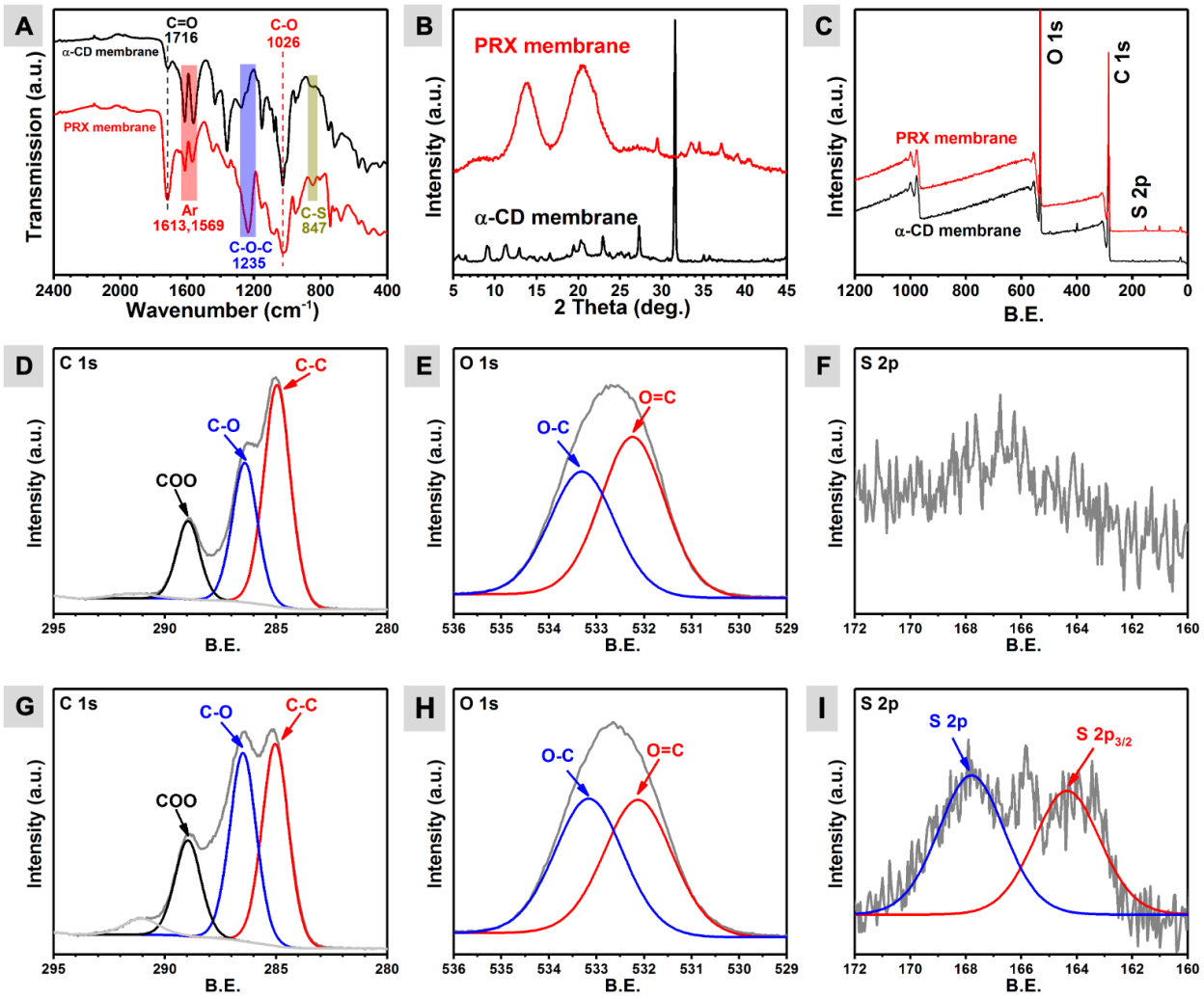

Fig. 3. (A) ATR-FTIR, (B) XRD, (C) wide scan XPS spectra of CD and PRX-4k membranes. High-resolution XPS spectra of the (D-F) CD and (G-I) PRX-4k membranes.

X-ray diffraction (XRD) was then used to examine the structural changes of the *α*-CD membrane after the inclusion of PEG. The pristine *α*-CD membrane exhibited a channel-type packing structure with two characteristic peaks in the regions of 10.5°-13.5° and 18.5°-21.5° (Fig. 3B) [24]. Importantly, these salient peaks become broader after the inclusion of PEG, indicating changes to the channel-type within *α*-CD. ATR-FTIR analysis of the prepared PRX-4k membrane after PEG complexation and end-capping showed a strong peak at 1235 cm^{-1}, and a weaker peak at 847 cm^{-1}, corresponding to the C-O-C vibration of the PEG backbone and the C-S vibration of the end-capping reagent, respectively (Fig. 3B). To further confirm both the complexation of PEG into the CD layer and the successful end-capping, the complete PRX-4k membrane was characterized by X-ray photoelectron spectroscopy (XPS) (Fig. 3C-I). Both the CD and PRX membranes show spectra characteristic of C 1s and O 1s. The peaks at 284.6, 286.5 and 288.7 eV correspond to the C–C, C–O and (C=O)O bonds in the membrane structure, respectively (Fig. 3D and G), while the peaks at 532.1 and 533.4 eV can be attributed to the O=C and O-C bonds, respectively (Fig. 3E and H). The decreased C-C/C-O peak intensity ratio in the PRX membrane is further evidence for successful PEG complexation with CD. Importantly, the PRX-4k membrane presents the characteristic S 2p peaks at 164.2 and 167.8 eV, corresponding to S $2p_{3/2}$ and S 2p, respectively (Fig. 3I) [25, 26], whereas no S 2p spectra were detected in CD membranes (Fig. 3F), further confirming successful end-capping *via* the thiol-yne reaction.

3.2 Nanofiltration performance

Following the successful fabrication of PRX-based nanofiltration membranes, we next examined their performance in the separation of organic molecules and inorganic heavy metal ions from solution. For several solvents, the α-CD membranes display a higher solvent permeance (*e.g.* H_2O permeance >16 L h^{-1} m^{-2} bar^{-1}, Fig. 4A) compared with previously reported β-CD membranes (~11 L h^{-1} m^{-2} bar^{-1}) [16]. This effect may be attributed to the reduced thickness (*ca.* 170 nm) of the membranes explored here, despite their higher apparent thickness resulting from the observed wrinkled morphology. Interestingly, each of the fabricated membranes exhibited significantly higher methanol permeance than water permeance. This may be due to the lower polarity of methanol, leading to weaker interactions between methanol and the α-CD and/or PEG membrane materials. This effect resulted in a fast penetration rate for methanol, in agreement with previous reports [27]. Both the α-CD cavities and the crosslinking sections between α-CDs contribute to the filtration properties. As expected, the solvent permeance of the α-CD membranes is higher than those of all PRX membranes, due to the relatively large free volume contributed by the cavities of pristine CDs and inter CD spaces. As a result, the resultant CD membranes display lower rejection rates toward 4-(phenylazo)benzoic acid (PBA (MW=226.23 g mol^{-1}), 18.7%, Fig. 4B) and inorganic metal ions (*e.g.* $CuSO_4$•$5H_2O$: 12.8%, Table 1).

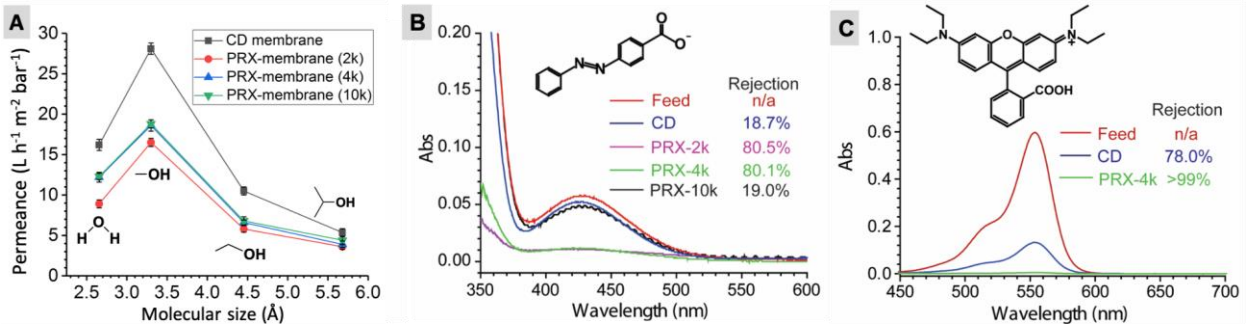

Fig. 4. (A) Pure solvent (water, methanol, ethanol, and isopropanol) permeance *versus* molecular diameter through CD and PRX (PEG inclusion: 2,000, 4,000, 10,000 g mol^{-1}) membranes. The

solvent molecular diameter is referred from Ref. [28]. (B-C) Rejection rates of 4-(phenylazo)benzoic acid (PBA, feed = 10 ppm) and rhodamine B (RB, feed = 2.5 ppm) by the CD and PRX-4k membranes. The applied low feed concentrations of PBA and RB tested here were selected to ensure an accurate quantitation *via* UV-Vis analysis.

Assessment of the PRX membranes highlighted that separation performance is significantly affected by the molecular weight of the complexed PEG. Specifically, the PRX-2k membranes display the lowest solvent permeance (Fig. 4A), while the PRX-10k membranes exhibit poor selectivity (rejection rates) of PBA (Fig. 4B). In addition, we observed that despite the PRX-4k and 10k membranes exhibiting similar solvent permeation rates, the PRX-4k membrane shows a much higher PBA rejection rate than that of PRX-10k membranes (80.1% *vs.* 19.0%, Fig. 4B). In the reaction mixture, PEG chains with different molecular weights will form random coils with different hydrodynamic diameters. The larger the diameter, the more difficult it is to form inclusion complexation. Thus, we attribute this to the difference in PEG inclusion ratio. Complexation with PEG of lower molecular weight results in a higher inclusion ratio into the CD cavities, through which a denser PRX membrane was prepared with much reduced inter-/intra- CD spaces and solution/solute diffusion pathways, and *vice visa*. Therefore, we observed that PEG with an intermediate molecular weight of 4,000 g mol^{-1} can induce a suitable degree of inclusion complexation to yield a PRX membrane with both good permeance and high rejection rates.

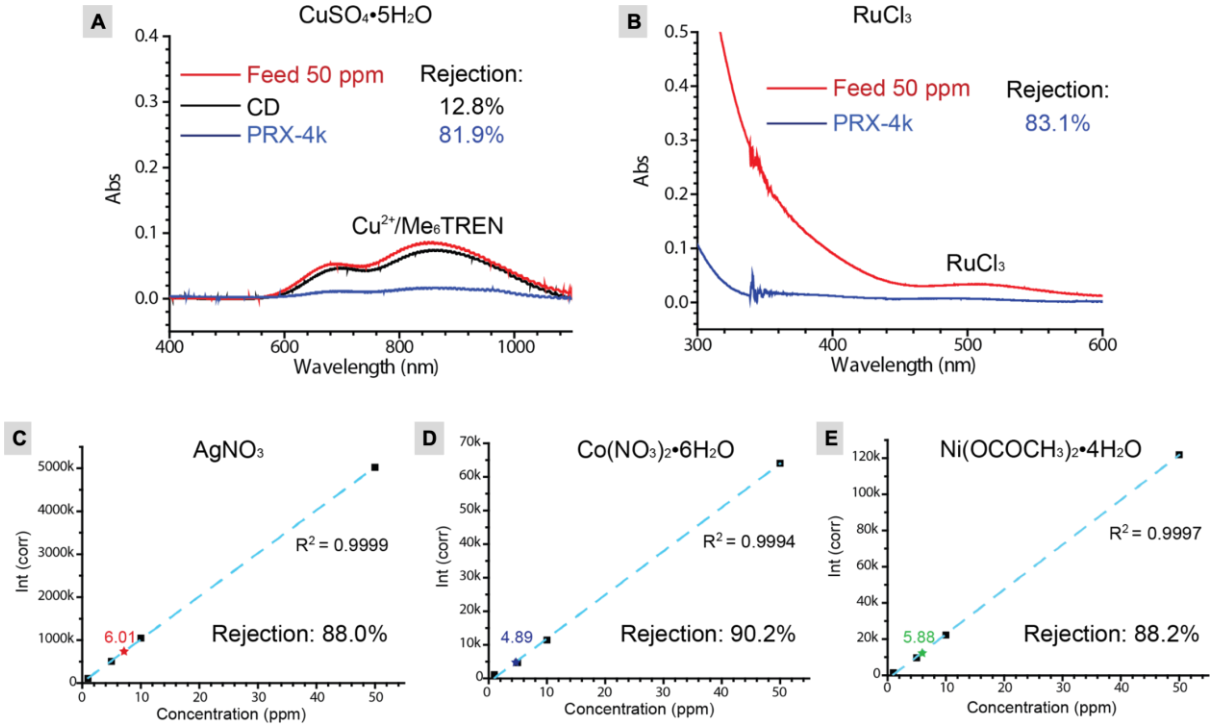

Fig. 5. The separation performance of PRX-4k membranes towards inorganic metal ions.

Further filtration assessment of the PRX-4k membranes suggested an excellent rejection rate of rhodamine B (MW=479.01 g mol^{-1}; >99%) together with good water permeance (7.1 L h^{-1} m^{-2} bar^{-1}) (Fig. 4C and Table 1). Such separation performance has not been achieved using pristine CD membranes and is superior to that of most state-of-the-art nanofiltration membranes listed in Table S1 [5]. Considering the high separation performance of PRX-4k membranes in the separation of solvents and organic molecules, they were further challenged in the separation of inorganic metal ions for potential water nanofiltration applications. Notably, the PRX-4k membranes show good water permeance (5.9 L h^{-1} m^{-2} bar^{-1}), as well as high rejection rates (>80%) for all metal salts examined here (Fig. 5 and Table 1). The highest rejection rates were observed for $Co(NO_3)_2$•$6H_2O$ (>90%), highlighting the effectiveness of this technology. In addition, the PRX-4k membranes display highly stable separation performance, retaining their rejection rate towards Cu(II) after 9 sequential separations over 48 hours (Fig. 6).

Table 1. The summary of the H_2O permeance and rejection of various organic/inorganic molecules.

Membranes	Feed concentration (ppm)		Permeance[a]	Rejection
CD-membrane	4-(phenylazo)benzoic acid	10	8.1	18.7
	Rhodamine B	2.5	10.4	78.0
	$CuSO_4•5H_2O$	50	8.9	12.8
PRX-4k membrane	4-(phenylazo)benzoic acid	10	5.8	80.1
	Rhodamine B	2.5	7.1	>99
	$CuSO_4•5H_2O$	50	6.3	80.2
	$RuCl_3$	50	5.9	83.1
	$AgNO_3$	50	5.5	88.0
	$Co(NO_3)_2•6H_2O$	50	5.9	90.2
	$Ni(OCOCH_3)_2•4H_2O$	50	6.2	88.2

[a] The permeance and rejection rate were acquired after 2 hours test.

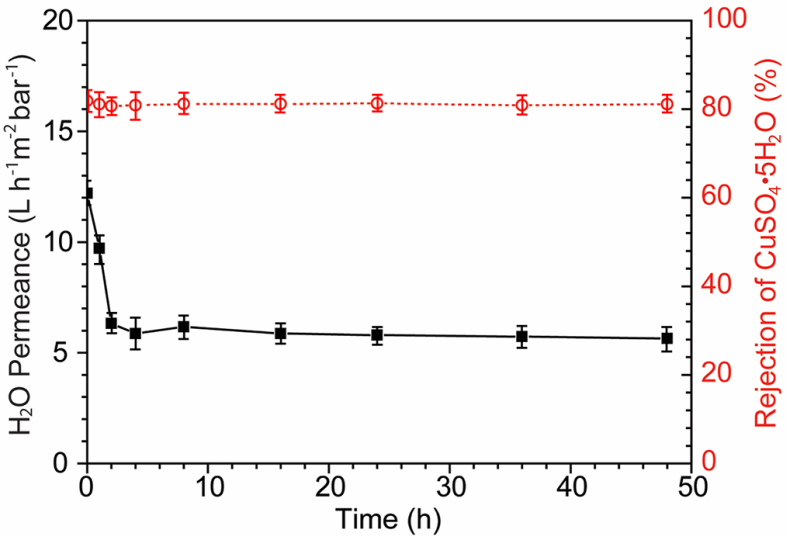

Fig. 6. The long-term H_2O permeance and rejection of $CuSO_4•5H_2O$ of PRX-4k membrane.

4. Conclusions

In summary, we developed a novel polyrotaxane-based composite nanofiltration membrane for high-performance size-selective molecular sieving. The PRX membranes are prepared *via* a novel, straightforward IP method, followed by *in-situ* PEG inclusion complexation and end-capping reaction. The resultant PRX membranes display an increased surface area with a PRX-film thickness of <200 nm, highly conducive to separation applications. The PRX-4k membrane combined the benefits of both high solvent permeance and excellent rejection rates for both organic dyes and heavy metal ions. The nanofiltration performance of the PRX membranes, along with their ease of scalability and excellent stability represent a promising new direction in the development of nanofiltration membranes.

Conflicts of interest

The authors declare no competing financial interest.

Acknowledgements

The authors appreciate the Bio21 Advanced Microscopy Facility for the assistance with material characterization and Mr. Nicolas Chan for the help of ATR-FTIR test. Min Liu acknowledges the support from China Scholarship Council - University of Melbourne Research Scholarship (No. 201606260063) and Particulate Fluids Processing Centre (PFPC). Qiang Fu acknowledges the Australian Research Council under the Future Fellowship (FT180100312).

Appendix A. Supplementary data

Supplementary data associated with this article can be found, in the online version.

References

[1] R. Connor, The united nations world water development report 2015: Water for a sustainable world, UNESCO Publishing, 2015.

[2] P. Marchetti, M.F. Jimenez Solomon, G. Szekely, A.G. Livingston, Molecular separation with organic solvent nanofiltration: a critical review, Chem. Rev., 114 (2014) 10735-10806.

[3] P. Vandezande, L.E. Gevers, I.F. Vankelecom, Solvent resistant nanofiltration: Separating on a molecular level, Chem. Soc. Rev., 37 (2008) 365-405.

[4] H.B. Park, J. Kamcev, L.M. Robeson, M. Elimelech, B.D. Freeman, Maximizing the right stuff: the trade-off between membrane permeability and selectivity, Science, 356 (2017) 1137.

[5] D.B. Shinde, G. Sheng, X. Li, M. Ostwal, A.-H. Emwas, K.-W. Huang, Z. Lai, Crystalline 2D covalent organic framework membranes for high-flux organic solvent nanofiltration, J. Am. Chem. Soc., 140 (2018) 14342-14349.

[6] H. Yang, L. Yang, H. Wang, Z. Xu, Y. Zhao, Y. Luo, N. Nasir, Y. Song, H. Wu, F. Pan, Covalent organic framework membranes through a mixed-dimensional assembly for molecular separations, Nat. Commun., 10 (2019) 2101.

[7] L. Valentino, M. Matsumoto, W.R. Dichtel, B.J. Mariñas, Development and performance characterization of a polyimine covalent organic framework thin-film composite nanofiltration membrane, Environ. Sci. Technol., 51 (2017) 14352-14359.

[8] K. Dey, M. Pal, K.C. Rout, S. Kunjattu H, A. Das, R. Mukherjee, U.K. Kharul, R. Banerjee, Selective molecular separation by interfacially crystallized covalent organic framework thin films, J. Am. Chem. Soc., 139 (2017) 13083-13091.

[9] X. Li, Y. Liu, J. Wang, J. Gascon, J. Li, B. Van der Bruggen, Metal-organic frameworks based membranes for liquid separation, Chem. Soc. Rev., 46 (2017) 7124-7144.

[10] Y. Li, L.H. Wee, A. Volodin, J.A. Martens, I.F. Vankelecom, Polymer supported ZIF-8 membranes prepared *via* an interfacial synthesis method, Chem. Commun., 51 (2015) 918-920.

[11] R.J. Petersen, Composite reverse osmosis and nanofiltration membranes, J. Membr. Sci., 83 (1993) 81-150.

[12] J.R. Holst, A. Trewin, A.I. Cooper, Porous organic molecules, Nat. Chem., 2 (2010) 915-920.

[13] H. Dodziuk, Cyclodextrins and their complexes: Chemistry, analytical methods, applications, John Wiley & Sons, 2006.

[14] P. Rölling, M. Lamers, C. Staudt, Cross-linked membranes based on acrylated cyclodextrins and polyethylene glycol dimethacrylates for aromatic/aliphatic separation, J. Membr. Sci., 362 (2010) 154-163.

[15] L. Yue, S. Wang, D. Zhou, H. Zhang, B. Li, L. Wu, Flexible single-layer ionic organic–inorganic frameworks towards precise nano-size separation, Nat. Commun., 7 (2016) 10742.

[16] L.F. Villalobos, T. Huang, K.V. Peinemann, Cyclodextrin films with fast solvent transport and shape-selective permeability, Adv. Mater., 29 (2017) 1606641.

[17] T. Huang, T. Puspasari, S.P. Nunes, K.V. Peinemann, Ultrathin 2D-layered cyclodextrin membranes for high-performance organic solvent nanofiltration, Adv. Funct. Mater., (2019) 1906797.

[18] Z. Yao, H. Guo, Z. Yang, W. Qing, C.Y. Tang, Preparation of nanocavity-contained thin film composite nanofiltration membranes with enhanced permeability and divalent to monovalent ion selectivity, Desalination, 445 (2018) 115-122.

[19] J. Xue, Z. Jiao, R. Bi, R. Zhang, X. You, F. Wang, L. Zhou, Y. Su, Z. Jiang, Chlorine-resistant polyester thin film composite nanofiltration membranes prepared with β-cyclodextrin, J. Membr. Sci., 584 (2019) 282-289.

[20] D.L. Gin, R.D. Noble, Designing the next generation of chemical separation membranes, Science, 332 (2011) 674-676.

[21] S. Tan, E. Nam, J. Cui, C. Xu, Q. Fu, J.M. Ren, E.H.H. Wong, K. Ladewig, F. Caruso, A. Blencowe, G.G. Qiao, Fabrication of ultra-thin polyrotaxane-based films *via* solid-state continuous assembly of polymers, Chem. Commun., 51 (2015) 2025-2028.

[22] S. Tan, Q. Fu, J.M. Scofield, J. Kim, P.A. Gurr, K. Ladewig, A. Blencowe, G.G. Qiao, Cyclodextrin-based supramolecular polymeric nanoparticles for next generation gas separation membranes, J. Mater. Chem. A, 3 (2015) 14876-14886.

[23] M.L. Bruschi, Strategies to modify the drug release from pharmaceutical systems, Woodhead Publishing, 2015.

[24] C.C. Rusa, T.A. Bullions, J. Fox, F.E. Porbeni, X. Wang, A.E. Tonelli, Inclusion compound formation with a new columnar cyclodextrin host, Langmuir, 18 (2002) 10016-10023.

[25] C.F. Edwards, W.P. Griffith, D.J. Williams, New thiosulfato complexes of osmium, J. Chem. Soc., Dalton Trans., (1992) 145-151.

[26] E. Kang, K. Neoh, X. Zhang, K. Tan, D. Liaw, Surface modification of electroactive polymer films by ozone treatment, Surf. Interface Anal., 24 (1996) 51-58.

[27] W. Zhang, L. Zhang, H. Zhao, B. Li, H. Ma, A two-dimensional cationic covalent organic framework membrane for selective molecular sieving, J. Mater. Chem. A, 6 (2018) 13331-13339.

[28] S. Kandambeth, B.P. Biswal, H.D. Chaudhari, K.C. Rout, S. Kunjattu H, S. Mitra, S. Karak, A. Das, R. Mukherjee, U.K. Kharul, Selective molecular sieving in self-standing porous covalent-organic-framework membranes, Adv. Mater., 29 (2017) 1603945.

For TOC only

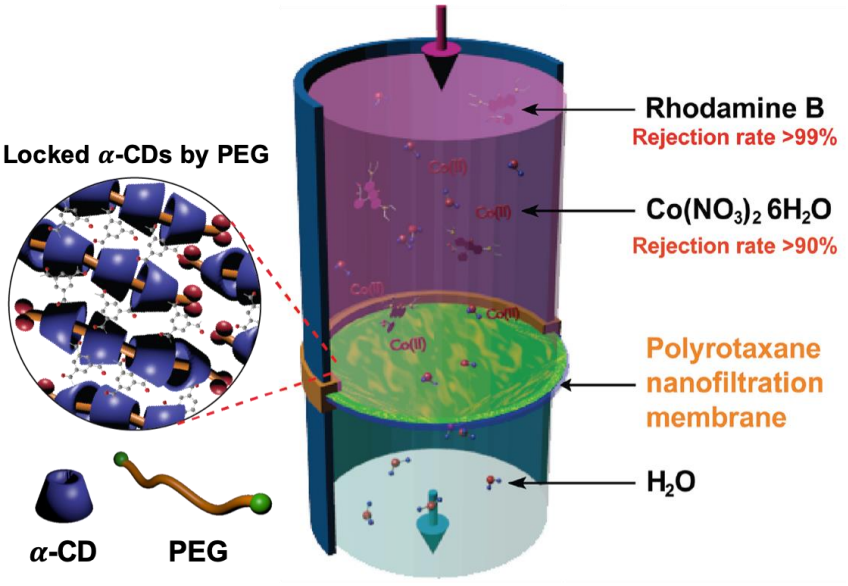
Locked α-CDs by PEG
α-CD
PEG
Rhodamine B
Rejection rate >99%
Co(NO3)2 6H2O
Rejection rate >90%
Polyrotaxane
nanofiltration
membrane
H2O